Available online at www.sciencedirect.com
SCIENCE DIRECT®
International Journal of Heat and Mass Transfer 47 (2004) 1997–2014
International Journal of HEAT and MASS TRANSFER
www.elsevier.com/locate/ijhmt

Influence of the magnetic field and the conductance ratio on the mass transfer rotating lid driven flow

A. Kharicha *, A. Alemany, D. Bornas

Pamir Team of the Laboratory LEGI, BP53, 38041 Grenoble Cedex 9, France

Received 28 May 2002

Abstract

A numerical study of a steady laminar magnetohydrodynamic (MHD) flow driven by a rotating disk at the top of a cylindrical cavity filled with a liquid metal is presented. The fluid flow field was calculated using a finite volume computational fluid dynamics (CFD) model. The effects of the magnetic field, the fluid and wall electrical conductivities, and the wall thickness are investigated. The relevant key parameters for the MHD flows are the Hartmann number M, and the Reynolds number Re. The study was performed for various $Re \geqslant 100$ *and* for M in the range $0 \leqslant M \leqslant 100$. This corresponds to a range of interaction parameter $N = M^2/Re$ of $0 \leqslant N \leqslant 100$. Here the magnetic Reynolds number R_m is assumed to be very small but the small-induced magnetic field was taken into account in the formulation of the problem. The work focuses on thin walls, which simplifies the boundary conditions. The thin wall boundary condition is used for the first time for a moving wall. It is shown that for fixed values of the Hartmann and Reynolds numbers, the velocity distribution depends strongly on the conductance ratio k, in spite of the fact that, the Hartmann layer thickness and side layer thickness do not vary with k. The numerical model is also applicable to non-MHD flows, and gives good agreement with previous experiments. The study is destined to predict the influence of a magnetic field on the corrosion rate of a liquid metal on a metallic wall. The results are devoted to analyse the corrosion processes of stainless steels by the Pb–17Li liquid alloy for the fusion reactor. It is assumed that this corrosion is controlled by the near-wall hydrodynamic which is then controlled by an external magnetic field. The concentration equation for the corrosion product is solved, and predicts the evolution of the mass transfer with M. At same magnitude of M the mass transfer is higher for conducting than insulating walls.

1. Introduction

In the water-cooled blankets for fusion reactors, which use a strong magnetic field to confine the plasma, the liquid alloy Pb–17Li has been proposed as breeder material. During operation, structural materials constituting the duct wall of the blanket, such as austenitic and martensitic steels, exposed to Pb–17Li are subject to corrosion [1]. The corrosion depends on factors such as time, temperature, liquid and solid compositions, thermal gradients and hydrodynamics. As in electrochemistry, it is expected that this last parameter can greatly affect the mass transfer from the solid to the liquid phase via the velocity gradient at the solid–liquid interface. It is also well known that a magnetic field changes the velocity distribution in liquid metal duct flows. Therefore, corrosion of steels exposed to flowing Pb–17Li may be modified by the magnetic field used to confine the plasma.

The confirmation of this magnetic field hypothesis requires an accurate knowledge of the correlation between hydrodynamics in a magnetic field and the rate of the mass transfer. To achieve that goal, an experiment will be performed to measure the corrosion of a rotating electrode (of the same material which will be used for the blanket) generating a re-circulating motion in a cylindrical cavity subjected to a strong magnetic field. The influence of a magnetic field on the electrodepositing mass transfer processes is well known from the

* Corresponding author.

0017-9310/$ - see front matter © 2003 Published by Elsevier Ltd.
doi:10.1016/j.ijheatmasstransfer.2003.02.001

Nomenclature

B_0	axial imposed magnetic field [T]
b_θ^*	induced tangential magnetic field [T]
b_θ	dimensionless induced tangential magnetic field [–]
D	diffusivity of the corrosion product [m^2/s]
e_w	wall thickness [m]
$\vec{F}$	Lorentz force [$kg\,m/s^2$]
H	height of the cylinder (see Fig. 1) [m]
k	conductance ratio [–]
M	Hartmann's number [–]
N	interaction parameter [–]
j_r	radial electric current [A/m^2]
j_z	axial electric current [A/m^2]
j_θ	tangential electric current [A/m^2]
J_r	dimensionless radial electric current [–]
J_z	dimensionless axial electric current [–]
J_θ	dimensionless axial electric current [–]
I_t	dimensionless total current [–]
p^*	pressure [$kg/(m\,s^2)$]
P	dimensionless pressure [–]
R	radius of the cylinder (see Fig. 1) [m]
Re	Reynolds number [–]
R_m	magnetic Reynolds number [–]
r^*	radial coordinate [m]
r	dimensionless radial coordinate [–]
Sc	Schmidt number [–]
Sh	Sherwood number [–]
u_r	radial velocity [m/s]
u_θ	azimuthal velocity [m/s]
u_z	axial velocity [m/s]
U_r	dimensionless radial velocity [–]
U	dimensionless axial velocity [–]
U_θ	dimensionless azimuthally velocity [–]
z^*	height coordinate [m]
z	dimensionless height coordinate [–]

Greek symbols

v	kinematic viscosity [$m^2\,s^{-1}$]
μ	magnetic permeability [$kg^{-1}\,m^{-1}\,s^{-1}$]
ρ	fluid density [$kg\,m^{-3}$]
σ_f	fluid electrical conductivity [$\Omega\,m^{-1}$]
σ_w	wall electrical conductivity [$\Omega\,m^{-1}$]
Ω	rotating disk angular velocity [$rad\,s^{-1}$]
ω	core flow angular velocity [$rad\,s^{-1}$]
φ	dimensionless electric potential [–]
Ψ	dimensionless electric streamfunction [–]
δ	Hartmann's layer thickness [–]
$\delta_\parallel$	parallel layer thickness [–]
Δ	Laplacian operator
Δr	grid increment in the radial direction [–]
Δz	grid Increment in the axial direction [–]

electrochemists [2–4] and from the crystal growth specialists [5,6]. Considering the simple geometry used to perform experimental tests, the first step of this work is to determinate the flow pattern in such a cavity. Numerous papers have been published on the study of a viscous liquid flow driven by one or two rotating disks without magnetic field [7–9]. The cases of a disk driven flow in a cylindrical enclosure mainly focus on small aspect ratio ($H/R \ll 1$) [10], this configuration being more representative of the structure of many hydraulic machines (turbines, centrifugal pumps, etc.). When the aspect ratio is greater than 1, as in the present work ($H/R = 2$), the influence of the lateral walls on the flow can no longer be neglected. The corresponding magnetohydrodynamic (MHD) problem has not been studied in detail up to now. Only two papers could be found in the literature [11,12], and both cover describe asymptotic flow solutions with a strong axial magnetic field.

The present work describes the numerical analysis used to predict the velocity distribution in a cylindrical cavity with a rotating end wall under an axial magnetic field. It is shown that the velocities depend on the thickness and the electrical conductivity of the walls. For thin walls the significant parameter is the conductance ratio k, the ratio of the wall conductance to the liquid metal conductance. Bessaih et al. [11] have only investigated the simple cases of an electrically insulating wall ($k = 0$) and a perfectly conducting wall ($k = +\infty$). But, according to Molokov [13,14] the conductance ratio k has a very high influence on the flow pattern. The present work demonstrates the influence of the wall properties (thickness and electrical conductivity) on the velocity distribution. In a second part, the distribution of the velocity in the cavity is used to solve the convection diffusion equation which is assumed to control the mass transfer rate. Consequently, the influence of the magnetic field on the corrosion rate will be analysed through the modification of the flow configuration inside the cavity.

2. Formulation of the hydrodynamics problem

Let us consider an incompressible, viscous, and electrically conducting fluid contained in a cylindrical cavity of radius R (Fig. 1) submitted to an axial magnetic field B_0. The top wall of the cavity is rotating with an angular velocity Ω are constant. The fluid properties as

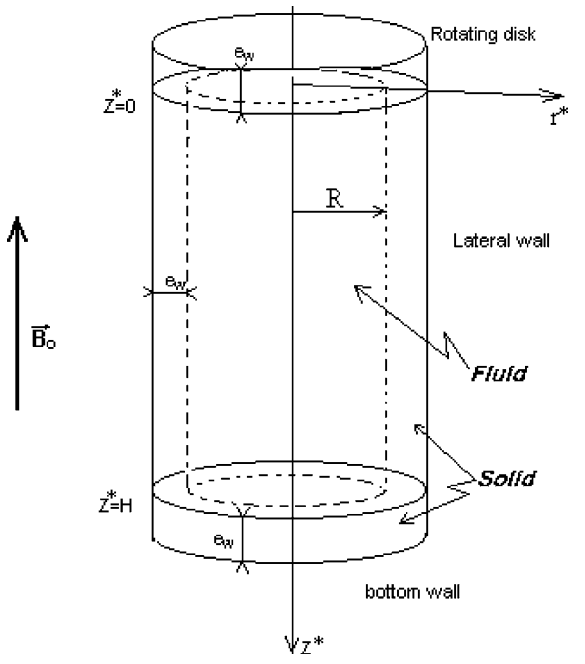

Fig. 1. Geometry of the considered problem. Because of the thin wall hypothesis the solid regions is not included in the calculation domain.

density (ρ), kinematics viscosity (ν), and electrical conductivity (σ_f) are assumed to be constant. The magnetic permeability (μ) is the same everywhere ($\mu = \mu_0$). All walls of the cavity have the same thickness (e_w) and electrical conductivity (σ_w).

The problem is expressed in cylindrical coordinates (r^*, θ, z^*) under the hypothesis of axial symmetry ($\partial/\partial\theta = 0$) and stationary flow condition ($\partial/\partial t = 0$). The magnetic Reynolds number, with a typical velocity V_0 defined latter, is small ($R_m = \sigma_f \mu V_0 R \ll 1$), so that the applied magnetic field B_0 is not significantly affected by the induced magnetic field $\vec{b}^*(b_r^*, b_\theta^*, b_z^*)$ which is generated in the fluid by the induced electric current $\vec{j}(j_r, j_\theta, j_z)$. Consequently, to the first order the Lorentz force applied to the flow can be written as

$$\vec{F} = \vec{j} \times \vec{B}_0 = \begin{cases} B_0 j_\theta, \\ -B_0 j_r, \\ 0. \end{cases} \tag{1}$$

Here $\vec{j}$ can be expressed from Ampere's relation as

$$\nabla \times \vec{b}^* = \mu \vec{j} \tag{2}$$

or, from the Ohm's law to first order, which consists of neglecting the induced magnetic field

$$\vec{j} = \sigma_f (\vec{E}^* + \vec{u} \times \vec{B}_0). \tag{3}$$

Here $\vec{E}^*$ is the induced electric field. The electric current which controls the Lorentz force, is deduced from Eqs. (2) or (3) as

$$\vec{j} = \begin{cases} j_r = -\dfrac{1}{\mu}\dfrac{\partial b_\theta^*}{\partial z^*} = -\dfrac{1}{\mu}\dfrac{1}{r^*}\dfrac{\partial}{\partial z^*}(r^* b_\theta^*), \\ j_\theta = -\sigma_f B_0 u_r, \\ j_z = \dfrac{1}{\mu}\dfrac{1}{r^*}\dfrac{\partial}{\partial r^*}(r^* b_\theta^*). \end{cases} \tag{4}$$

It is clear from Eq. (4) that the tangential component of the induced magnetic field, i.e. b_θ^*, appears as the stream function of the radial and axial component of the induced electric current, j_r, j_z. The expression for j_θ is deduced preferentially from the Ohm's law by taking into account that the azimuthally component of the electric field, $E_\theta^* = -\frac{1}{r^*}\frac{\partial \varphi}{\partial \theta}$, where φ is the electric potential, vanishes under the axial symmetry. Consequently, using the formulation (4), only the tangential component of the induced magnetic field is relevant to the description of the problem. This component can be deduced from the induction equation written to the first order as

$$B_0 \frac{\partial u_\theta}{\partial z^*} + \frac{1}{\mu\sigma_f}\left(\Delta b_\theta^* - \frac{b_\theta^*}{r^{*2}}\right) = 0. \tag{5}$$

On the hydrodynamic point of view, the problem is governed by the classical Navier–Stokes equations

$$U_r \frac{\partial U_r}{\partial r^*} + u_z \frac{\partial u_r}{\partial z^*} = -\frac{1}{\rho}\frac{\partial p^*}{\partial r^*} + \nu\left(\Delta u_r - \frac{u_r}{r^{*2}}\right) - \frac{1}{\rho} B_0 J\theta + \frac{u\theta^2}{r^*}, \tag{6}$$

$$u_r \frac{\partial u_\theta}{\partial r^*} + u_z \frac{\partial u\theta}{\partial z^*} = \nu\left(\Delta u\theta - \frac{u\theta}{r^{*2}}\right) - \frac{1}{\rho} j_r \cdot B_0 - \frac{u\theta u_r}{r^*}, \tag{7}$$

$$u_r \frac{\partial u_z}{\partial r^*} + u_z \frac{\partial u_z}{\partial z^*} = -\frac{1}{\rho}\frac{\partial p^*}{\partial z^*} + \nu \Delta u_z \tag{8}$$

and by the continuity equation

$$\frac{\partial}{\partial r^*}(r^* u_r) + r^* \frac{\partial u_z}{\partial z^*} = 0. \tag{9}$$

The set of equations (4)–(9) will be used to describe the flow configuration inside the cavity. (10) is the mass transfer coefficient which will be computed when the hydrodynamic will be known. By choosing the following characteristic typical scales: for the length $l_0 \sim R$, for the velocity $V_0 \sim \nu/R$, for the electric current density $J_0 \sim \sigma_f V_0 B_0$, for the pressure $P_0 \sim \rho V_0^2$, and for the magnetic field $b_0 \sim \mu\sigma_f V_0 B_0 R = R_m B_0$ and by using the following dimensionless parameters: $r = r^*/R$, $z = z^*/R$, $\vec{U}(U_r, U_\theta, U_z) = \vec{u}(u_r, u_\theta, u_z) \cdot R/\nu$, $p = p^*/(\rho V_0^2)$ and $b_\theta = b_\theta^*/(B_0 R_m)$; the dimensionless equations that control the flow field take the form

$$U_r\frac{\partial U_r}{\partial r}+U_z\frac{\partial U_r}{\partial z}=-\frac{\partial P}{\partial r}+\left(\Delta U_r-\frac{U_r}{r^2}\right)-M^2\cdot U_r+\frac{U_\theta^2}{r}, \tag{10}$$

$$U_r\frac{\partial U_\theta}{\partial r}+U_z\frac{\partial U_\theta}{\partial z}=\left(\Delta U_\theta-\frac{U_\theta}{r^2}\right)+M^2\cdot\frac{\partial b_\theta}{\partial z}-\frac{U_r\cdot U_\theta}{r}, \tag{11}$$

$$U_r\frac{\partial U_z}{\partial r}+U_z\frac{\partial U_z}{\partial z}=-\frac{\partial P}{\partial z}+\Delta U_z, \tag{12}$$

$$\frac{\partial}{\partial r}(rU_r)+r\frac{\partial U_z}{\partial z}=0, \tag{13}$$

$$\frac{\partial U_\theta}{\partial z}+\left(\Delta b_\theta-\frac{b_\theta}{r^2}\right)=0. \tag{14}$$

In this set of equations, the components of the current density have been replaced by their expressions deducted from (4). The problem seems to be controlled only by the Hartmann number $M=B_0R(\sigma_f/\nu)^{1/2}$, the ratio of electromagnetic force to the viscous force. In fact, due to the choice of the typical scales, the Reynolds number appears only in the expression for the boundary conditions (cf. (15)) and the magnetic Reynolds number only in the expression for the induced magnetic field ($b_\theta=b_\theta^*/(B_0R_m)$). The mass transfer is controlled by the Schmidt number $Sc=\nu/D$.

Two others parameters control the structure of the flow:

- The aspect ratio H/R, see Fig. 1. This study will be focused mainly on $H/R=2$ corresponding to the available facility.
- The electric properties of the walls taken into account by the conductance ratio $k=\sigma_w e_w/\sigma_f R$ to be introduced later in the electric boundary conditions.

The interaction parameter $N=M^2/Re$, the ratio of electromagnetic forces to inertial forces, is deducted from the Hartmann and Reynolds numbers.

3. The boundary conditions

3.1. Hydrodynamic conditions

The velocity field must satisfy the non-slip condition at the walls. These conditions are summarized by:

- At the surface of the rotating disk ($z=0$)

$$U_r=U_z=0,\quad U_\theta(r)=r\cdot\Omega/V_0=Re\cdot r. \tag{15}$$

- On the lateral and bottom walls of the cavity,

$$U_r=U_\theta=U_z=0. \tag{16}$$

- In addition, from the symmetry on the axis of the cavity ($r=0$):

$$\frac{\partial U_r}{\partial r}=\frac{\partial U_z}{\partial r}=0,\quad U_\theta=0. \tag{17}$$

3.2. Boundary conditions for the induced magnetic field

The closure of the electric current depends strongly on the wall electric properties (thickness and conductivity). Consequently, the Lorentz force and the velocity distribution are governed by these properties. Depending on the thickness, electrical conductivity, and magnetic permeability of the walls, numerous possible combinations of hydrodynamic and electromagnetic boundary conditions can be written. The electromagnetic boundary conditions depend on the conductivity ratio and the ratio of the wall thickness to the fluid radius R. In the general case these two ratios do not play the same role, but when the wall thickness is much smaller than the radius of the cavity, the expression for the boundary conditions is simplified. In the present work only the electric properties are taken into account and the focus is on thin walls. As will be demonstrated below, the thin wall hypothesis avoids having to solve the induction equation (14) in the solid media.

The thin wall hypothesis assumes that the electric potential does not vary across the wall; this means that the wall current density is tangential to the wall. In this case the significant parameter is the conductance ratio $k=\sigma_w e_w/\sigma_f R$, thus the wall thickness (e_w) and wall conductivity (σ_w) play a similar role. The thin wall has never been used for a moving wall, the boundary conditions at the rotating lid has to be established.

Let us consider the interface between the rotating disk and the liquid metal. The magnetic boundary conditions can be deducted from the conservation of the electric current between the fluid and a circular corona of the wall of dimensionless size dr, thickness e_w/R and radius r (Fig. 2). The vertical component of the current

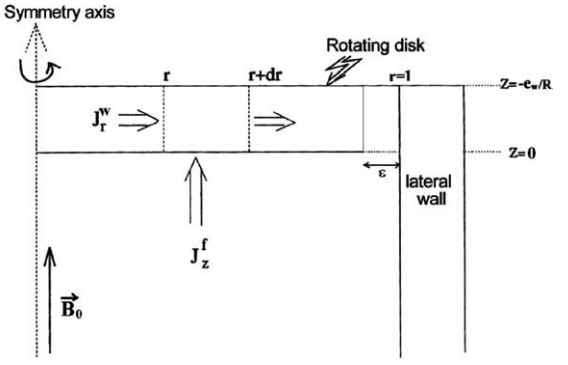

Fig. 2. The closure of the electric current in the rotating disk.

density J_z in the fluid, at the interface with the disk has to close inside the thickness of the disk, causing a change in the radial component J_r of the electric current. By using respectively the superscripts (w) and (f) for the wall and the fluid, the electric conservation equation is

$$J_z^{\mathrm{f}} = -\frac{e_{\mathrm{w}}/R}{r}\frac{\partial}{\partial r}(rJ_r^{\mathrm{w}}). \tag{18}$$

The continuity of the electric potential at the wall imposes the continuity of the radial component of the electric field. That means that at the disk surface:

$$\forall r : E_r^{\mathrm{w}} = E_r^{\mathrm{f}}. \tag{19}$$

Consequently, taking into account of the Ohm's law (3),

$$\forall r : \frac{J_r^{\mathrm{w}}}{\sigma_{\mathrm{w}}/\sigma_{\mathrm{f}}} = J_r^{\mathrm{f}}. \tag{20}$$

The rotating velocity of the upper disk closing the cavity is implicitly taken into account in the formulation of the problem. For J_r^{f} using the continuity equation ($\vec{\nabla}\cdot\vec{J} = 0$), Eq. (18) gives:

$$J_z^{\mathrm{f}} = k\frac{\partial}{\partial z}(J_z^{\mathrm{f}}). \tag{21}$$

The dimensionless form of the Eq. (4) combined with Eq. (21) gives:

$$\forall r : \frac{\partial(rb_\theta)}{\partial r} = k\frac{\partial}{\partial z}\left(\frac{\partial(rb_\theta)}{\partial r}\right). \tag{22}$$

By integrating between $r = 0$ and r we obtain the final expression for the magnetic boundary condition at the disk interface

$$b_\theta = k\frac{\partial}{\partial z}(b_\theta). \tag{23}$$

As it can be see the mobility of the rotating disk does not induce a modification of the boundary condition. This is connected to the no slip boundary condition for the velocity between the two media. At the others walls, using the same procedure as for the rotating disk, we obtain:

- For the boundary condition at the bottom wall

$$b_\theta = -k\frac{\partial}{\partial z}(b_\theta) \tag{24}$$

- and for the lateral wall

$$b_\theta = -k\frac{1}{r}\frac{\partial(rb_\theta)}{\partial r}. \tag{25}$$

Thus, all the electric boundary conditions at the solid–fluid interface can be expressed by a general relation of the form

$$b_\theta = \chi\frac{\partial b_\theta}{\partial n}, \tag{26}$$

where n is the vector normal to the wall into the liquid, and χ is a function of k. By using relation (26) the calculation of the induced magnetic field is not necessary in the wall media for thin walls hypothesis. Thus the problem needs to be solved only in the conducting liquid. On the experimental point of view, the electric contact between the rotating disk and the lateral part of the cavity, which is not moving, can be considered with attention. Inside this gape (of size $\varepsilon/R < 10^{-3}$), Fig. 2, the fluid is in a Couette configuration and the vertical gradient of velocity $\frac{\partial U_\theta}{\partial z}$ is null along the depth of the rotating disk. Consequently there is no source to be added for the induction equation of b_θ. The modelling of real case can easily be done by changing the conductance ratio of the lid by $k = e_{\mathrm{w}}/R$ for $1 - \varepsilon/R \leqslant r \leqslant 1$. It is assumed this has a small influence on the global dynamic of the flow. The present study assumes a perfect contact between the rotating disk and the fix lateral walls.

The conductance ratio k plays a very important role in the velocity distribution. Generally the MHD flows have been treated only under the asymptotic conditions [11], the walls being either perfectly conducting ($k = \infty$) or insulating ($k = 0$). Using the present At the rotation axis of the disk, the symmetry conditions leads to

$$b_\theta(r = 0, z) = 0. \tag{27}$$

4. Numerical results and discussion

The numerical tool used, FLUENT, is a finite volume code coupled to a pressure correction equation based on the SIMPLEC algorithm. The different quantities associated with the set of equations are discretised on a unique rectangular grid and solved on the (r, z) plane. For the discretisation of spatial terms a second order UPWIND difference scheme was used. The solution in the meridian plane r–z was obtained as follows:

(a) Eq. (11) is first solved to get U_θ.
(b) b_θ is subsequently computed from Eq. (14).
(c) Next Eqs. (10), (12) and (13) are solved to get P, U_r and U_z.
(d) Steps (a) to (c) are repeated until convergence is obtained.

The increments Δr and Δz of the grid are not regular, in the Ekmann and Hartmann layers a strong refinement was made to solve the specific characteristic of the flow and to reduce the numerical errors. The grid used has

120×280 nodes and was chosen after performing grid tests. As mentioned before, when the Harmann number is sufficiently high ($M^2 > Re$), the flow configuration depends essentially on the interaction parameter that, for a fixed Re, varies from 0 to 100 in the present study. The velocity profiles are presented essentially for $Re = 100$, because the boundary layer profiles are better defined.

4.1. Solution without magnetic field

The problem has been investigated for different values of the aspect ratio H/R. The main conclusion is that the boundary layer at the rotating disk results from an equilibrium between the centrifugal and viscosity forces. The centrifugal force generates a high-pressure zone at the periphery of the rotating disk. This high-pressure zone entrains flow in the cavity that closes in the low-pressure zone on the axis. This phenomenon is well known as Ekmann pumping. When the Reynolds number is high enough to entrain all of the fluid contained in the cavity ($Re \geqslant 1000$), the calculations predict that the central core of the flow rotates with a constant angular velocity ω which depends only on the aspect ratio and not on the Reynolds number For small aspect ratios the result is $\omega \approx \Omega/3$, confirming the studies done by Lewellen [8] (Fig. 3). In contrast with the semi-analytical study by Tholman [7], when the aspect ratio becomes larger than 1, the ratio between the angular velocity of the disk and the angular velocity of the core flow seems to follow an asymptotic linear law $\Omega/\omega = 1 + 2 \cdot H/R$ (Fig. 3). This is confirmed experimentally by results extracted from Spohn [10,17] for different ratio aspects. In particular for H/R equal to 2, corresponding the present facility, there is an excellent agreement.

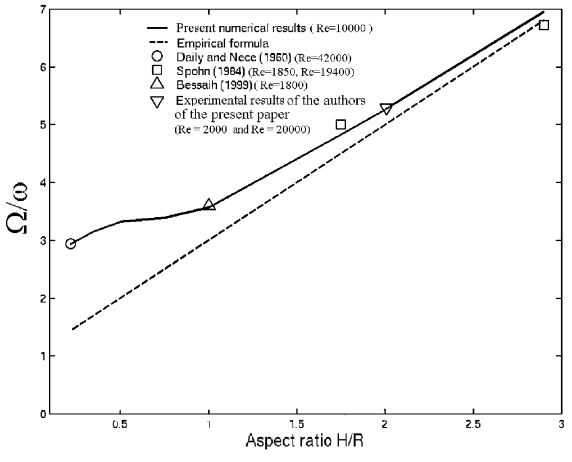

Fig. 3. Angular velocity ratio of the disk Ω to the core flow ω versus the aspect ratio for $M = 0$.

4.2. Solution with a magnetic field, insulating and perfectly conducting walls

The solutions without a magnetic field is used as the initial condition for the MHD case. As mentioned before, for high values of the Hartmann number the grid needs very strong refinement to yield good precision in the vicinity of the walls.

The cases of insulating and perfectly conducting walls have been investigated by Bessaih [11] only for asymptotic values of the Hartmann number, while the present study covers all values of this parameter. The method used by this author is different that used in the present paper. It is based on the electric potential distribution at the wall, while the present work uses the induced magnetic field. The comparison of results obtained with both methods (Fig. 4) does not show any difference, thus confirming the validity of the present approach.

For electrically insulating walls, the boundary conditions on the solid–fluid interfaces and on the axis have the simple form $b_\theta = 0$. The induced electric current lines characterised by the function $\psi = rb_\theta$, do not penetrate the walls and must close inside the conducting liquid, as shown in Fig. 5 for $M = 100$. The regions located just under the rotating disk and just above the bottom disk correspond to a concentration of the electric current lines perpendicular to the magnetic field B_0. As a result, in these locations the Lorentz force is large. Thus, when the Hartmann number increases, the Ekman layer characterised by an equilibrium between the centrifugal and viscous forces is progressively replaced by the Hartmann layer characterised by an equilibrium between electromagnetic and viscous forces. The analytic solution for large M calculated by Bessaih [11],

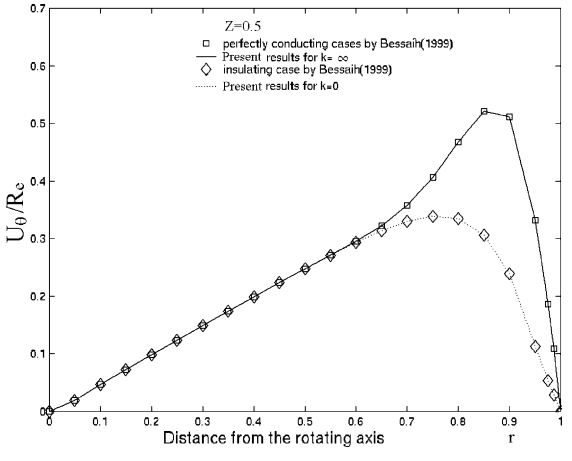

Fig. 4. Comparison between Bessaih's results and present results for perfectly conducting and insulating walls, $M = Re = 100$ and $H/R = 1$.

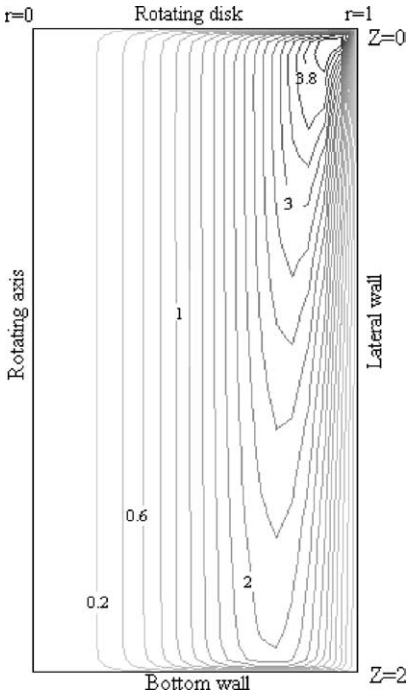

Fig. 5. Electric current streamlines for insulating walls ($Re = M = 100$). The iso-values of $(-\Psi)$ are indicated in the meridian plan (r, z).

shows that the flow is rotating as a rigid body at half of the velocity of the rotating disk, $U_\theta/Re = r/2$. For any Reynolds number in the range used in the present study, i.e. $0 < Re < 3500$, the asymptotic solution was reached for $M^2 > 50Re$ (Fig. 6). In these cases, the core flow is crossed by an almost axial electric current $J_z/R_e = \mathrm{O}(M^{-1})$ which closes through the top and the bottom Hartmann layers of thickness M^{-1}. Classically, the dimensionless total electric current in these Hartmann layers is on the order of unity. As a consequence in the core flow, the tangential component of the electromagnetic force vanishes. Then, in this region, the flow is characterised by equilibrium between the viscous driving stress from the disk at the top and the viscous braking at the bottom wall. This helps to understand why the core rotates at a velocity that is an exact average of the two ends walls.

For perfectly conducting walls, $k \to +\infty$; (Fig. 7) the tangential component of the current density in the fluid vanishes at the walls, and consequently the gradient of the tangential component of the induced magnetic field vanishes also, $\frac{\partial b_\theta}{\partial n} = 0$. Thus, close to both the rotating disk at the top and the fixed disk at the bottom, the current density and the magnetic field are parallel, the electromagnetic force vanishes, and this prevents the formation of the Hartmann layers. On the other hand and due to the fact that the current density is parallel to the magnetic field on both part of the cavity (at the top and at the bottom), the current density in the core flow is maintained also parallel to the magnetic field. In this case, the electromagnetic forces vanish everywhere, except at the vicinity of the lateral walls. Then under the diffusion processes, the viscosity influence becomes effective from the top to the bottom with a linear profile

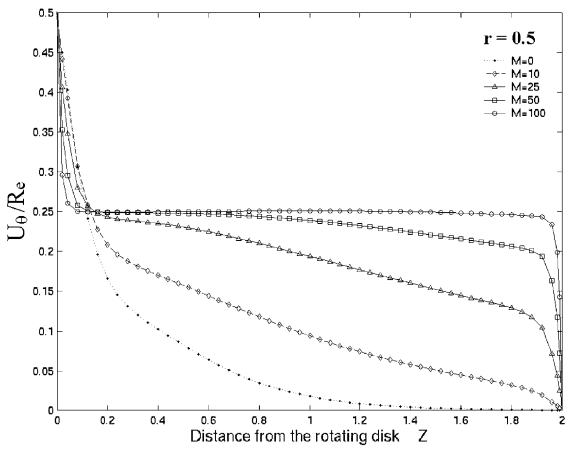

Fig. 6. Azimuthally velocity profiles for different Hartmann numbers ($Re = 100$) for insulating walls.

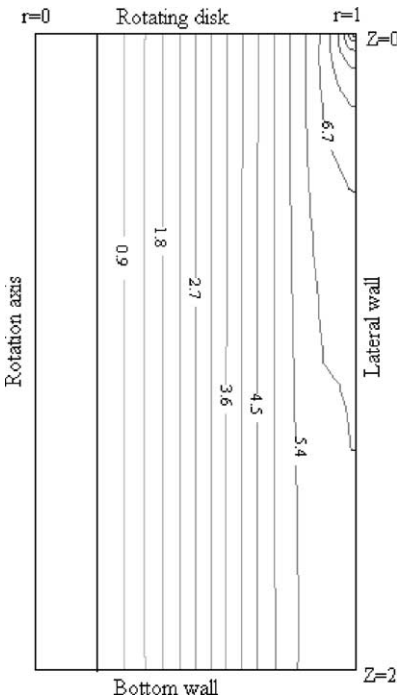

Fig. 7. Electric current streamlines for perfectly conducting walls ($M = Re = 100$).

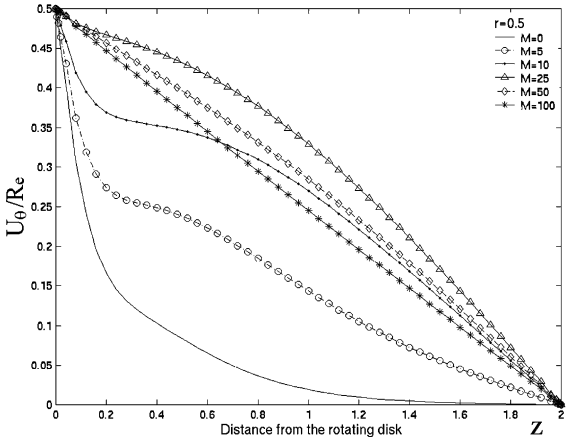

Fig. 8. Evolution of the azimuthally velocity for different values of the Hartmann number ($Re = 100$) for perfectly conducting walls.

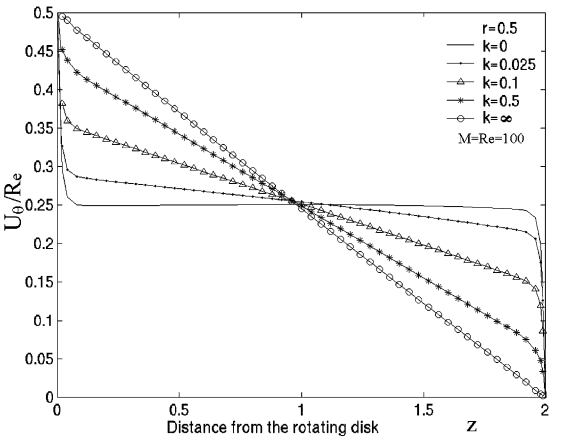

Fig. 9. Evolution of the azimuthally velocity along the $r = 0.5$ line, plotted for different values of the conductance ratio ($M = Re = 100$).

of the velocity distribution as in the classical Couette flow (Fig. 8). This explains the monotonous structure of the velocity field that varies linearly from the rotating disk value at the top to the zero fixed disk value at the bottom. For high values of the Hartmann number, the expression for the tangential velocity becomes

$$U_\theta/R_e = r(1 - z/2). \tag{28}$$

The asymptotic solution is also reached for $M^2 > 50Re$ (Fig. 8).

4.3. Solution with a magnetic field, arbitrary values of k

It is assumed that all walls (rotating and fixed) have the same conductance ratio k. The analysis is performed first for $Re = 100$ and $M = 100$, but for various values of k (Fig. 9). For this swirling flow it is convenient to distinguish between the azimuthally component of the velocity $(0, U_\theta, 0)$ and the meridian ones $(U_r, 0, U_z)$, the secondary flow, that can be characterised by streamlines.

It is well known that for strong magnetic fields, the flow splits into the following distinct sub-regions [14]:

1. The Hartman boundary layers adjacent to the rotating disk and the bottom wall with order (M^{-1}) thickness. They disappear when the walls are perfectly conducting.
2. The core flow between the Hartmann layers where the viscous effects are negligibly small.
3. The side layer, along the lateral wall of order $(M^{-1/2})$ thickness.

The azimuthally velocity profiles are strongly influenced by the conductance ratio (Fig. 9) and exhibit an almost linear variation versus the radius r (Fig. 10) except near the lateral wall.

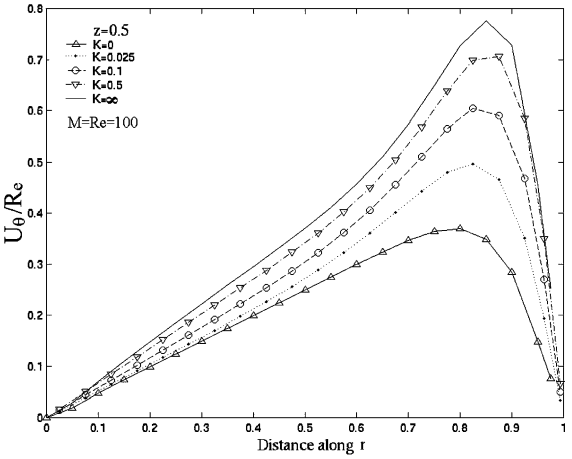

Fig. 10. The azimuthally velocity versus r along the $z = 0.5$ line, plotted for different values of the conductance ratio ($M = Re = 100$).

To interpret the numerical results, let us consider the asymptotic situations characterised by high values of the Hartmann number that allow neglecting the viscosity influence in the flow far from the lateral walls. The considered domain includes also the two Hartmann's layers at vicinity of the rotating and fix disks. The momentum equation (11) for the azimuthally velocity becomes

$$\frac{\partial^2 U_\theta}{\partial z^2} = -M^2 \frac{\partial b_\theta}{\partial z}. \tag{29}$$

According to Figs. 9–11, the solution for the velocity profile, respecting the boundary conditions at the wall (15)–(17), can be written in the form

$$U_\theta/R_e = r \cdot (\alpha \cdot z + \beta + (1 - \beta) \cdot \mathrm{e}^{-M \cdot z}). \tag{30}$$

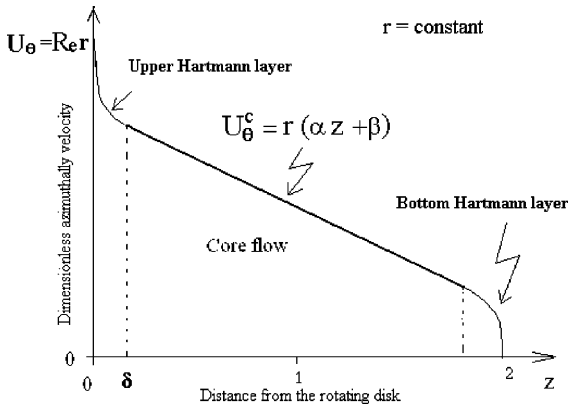

Fig. 11. Characteristic profile of the velocity in the axial direction. Both Hartmann layers are linked by the linear velocity profile U_θ^C of the core flow.

Here $r\cdot(\alpha\cdot z+\beta)=U_\theta^C/R_e$ (Fig. 11) is the linear core velocity. The coefficients α and β are unknown function of r and depend on the conductance ratio k. Neglecting the radial derivative of the velocity in (29) corresponds to neglect the radial component of the Laplacian of compared to the value of α. From Fig. 9 it can be deduced

$$U_\theta^C(r,z=1)=R_e\cdot r/2:\alpha+\beta=1/2. \tag{31}$$

For $M\gg 1$, α and β should, according to Fig. 9, have the values

$$k\to 0\Rightarrow\begin{cases}\alpha\to 0\\ \beta\to 1/2\end{cases}\quad\text{and}$$
$$k\to+\infty\Rightarrow\begin{cases}\alpha\to -1/2,\\ \beta\to 1.\end{cases} \tag{32}$$

These values corresponding to the insulating and perfectly conducting walls, will be taken as references for the general semi-analytic solution calculated in the following.

Replacing the velocity distribution corresponding to Eq. (30) in the asymptotic hydrodynamics equation (29) gives after a simple integration

$$b_\theta=r\cdot\frac{(1-\beta)\cdot R_e}{M}\cdot e^{-M\cdot Z}+b_\theta^C(r), \tag{33}$$

where b_θ^C is the induced magnetic field in the core. It can be determined from the induction equation (14) with U_θ and b_θ replaced by their semi-analytic forms (30) and (33) in the core flow, as

$$\alpha\cdot R_e\cdot r=-\frac{1}{r}\frac{\partial}{\partial r}\left(r\frac{\partial b_\theta^C}{\partial r}\right)+\frac{b_\theta^C}{r^2}$$
$$\Rightarrow\begin{cases}\alpha=0: & b_\theta^C=rR_e/2M,\\ \alpha\neq 0: & b_\theta^C=-\dfrac{\alpha R_e}{8}(r^3+C\cdot r).\end{cases} \tag{34}$$

For $\alpha=0$, the proposed expression for b_θ^C takes into account for the boundary condition for insulating walls ($b_\theta=0$). For $k\neq 0$, C is an unknown parameter which depends on the boundary condition at the limit of the core/Hartmann side layer. The essence of the parallel layer is that it provides a current path, in addition to that in the lateral wall. The parallel layer can be replaced by a wall of $M^{-1/2}$ conductance ratio. This consideration leads to a modification of the thin wall condition which, applied to b_θ^C in the form

$$b_\theta^C(r)=-(k+M^{-1/2})\frac{1}{r}\frac{\partial(rb_\theta^C(r))}{\partial r}, \tag{35}$$

is now applied to the core induced magnetic field b_θ^C. This kind of boundary conditions is commonly used in the literature [15] to allow the Hartmann and parallel layers to be left unresolved by the numerical grid while at the same time considering their joint effects due to the closure of the electric currents in the Hartmann layer and the wall. Putting (34) in (35), neglecting again the radial derivative of α compared to α, and applied at $r=1-M^{-1/2}\approx 1$ gives

$$\alpha\neq 0\Rightarrow C=-\frac{r^2\cdot(r+4\cdot(k+M^{-1/2})}{r+2\cdot(k+M^{-1/2})}$$
$$=-\frac{1+4\cdot(k+M^{-1/2})}{1+2\cdot(k+M^{-1/2})}. \tag{36}$$

To close this semi-analytic solution, it is necessary to express α and β by using the electric thin wall boundary condition (23) at the rotating disk written according to the expression (33) for b_θ

$$r\cdot\frac{(1-\beta)\cdot R_e}{M}-\frac{\alpha R_e}{8}(r^3+C\cdot r)$$
$$=k\cdot(1-\beta)\cdot r\cdot R_e\Rightarrow\beta=1-\frac{\alpha\cdot(r^2+C)}{8\cdot(k+1/M)}. \tag{37}$$

Using (31) we get the solution which verifies the references values (32), i.e.

$$k\neq 0\Rightarrow\begin{cases}\alpha=\dfrac{-1}{2(1-(r^2+C)/(8\cdot(k+1/M))},\\ \beta=\dfrac{1-(r^2+C)/(16\cdot(k+1/M))}{1-(r^2+C)/(8\cdot(k+1/M))}.\end{cases} \tag{38}$$

In Fig. 12 the semi-analytical solution for b_θ is compared to the numerical results for the induced magnetic field for two different values of k and for $Re=M=100$. The agreement for $r<0.6$ is good, in spite of the fact that the solution cannot be considered as completely asymptotic. In conclusion, it appears that the core induced magnetic field is constant along a vertical axis (Fig. 13). Since, according to the group of Eq. (4), the azimuthally component of the induced magnetic field can be interpreted as the stream function of the induced electric current, this explains why in the core, the electric

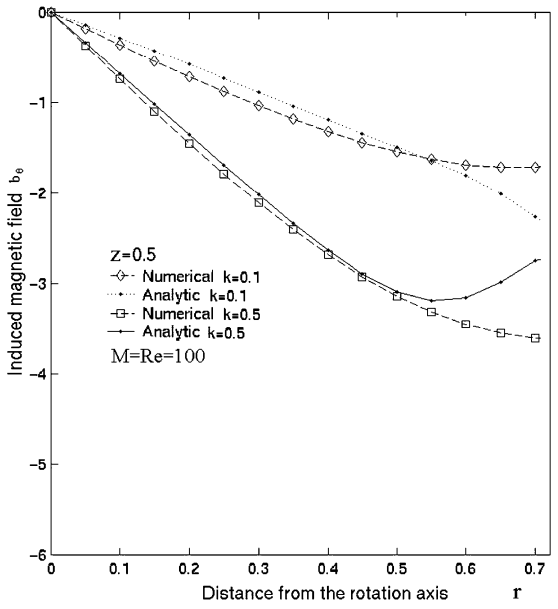

Fig. 12. Comparison of the semi-analytic theory for the core induced magnetic field b_θ^C with the numerical results, versus the radial coordinate for $z = 0.5$.

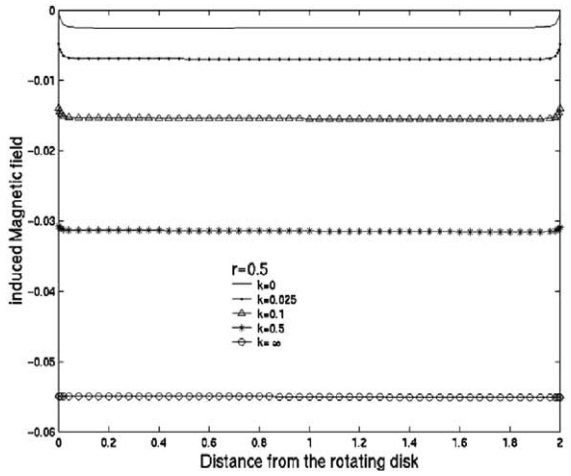

Fig. 13. Evolution of the induced magnetic field along $r = 0.5$ line, plotted for different values of the conductance ratio ($M = Re = 100$).

lines are parallel to the z axis (see Figs. 13 and 14). The comparison between the calculated values of α and β and the numerical results for a large range of k is given on Fig. 15; it show a very good agreement. On the other hand, the solution exhibits relatively small variations versus the distance from the rotation axis that according to Fig. 9 depends on the conductivity ratio k. From these results it can be noticed that, as in classical MHD

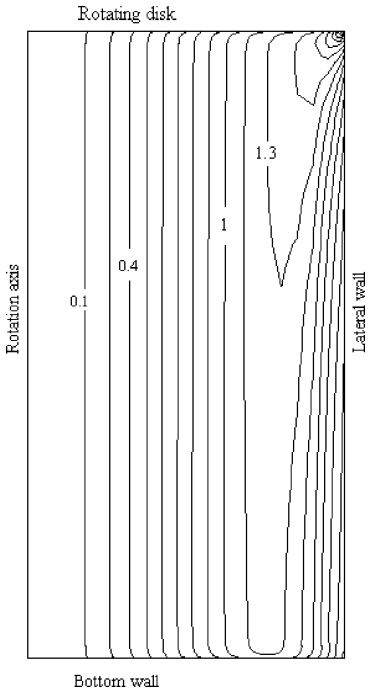

Fig. 14. Electric current streamlines for $k = 0.1$ ($Re = M = 100$). The iso-values of $(-\Psi)$ are indicated in the meridian plan (r, z).

problems, the Hartmann boundary layer thickness δ is constant versus k and disappears when the walls are perfectly conducting ($\alpha = -1/2,\ \beta = 1$) corresponding to $k = \infty$. The velocity distribution $U_\theta(r, z)$ inside the Hartmann layer is controlled by the intensity of the radial component of the electric current J_r, which is, according to Eq. (4) and the boundary condition (23), of $O(b_\theta/k)$. Consequently, the Lorentz' force in the azimuthally direction decreases when k increases and the viscosity diffuses the motion far from the disk. This explain the decreasing of the gradient of $U_\theta(r, z)$ just under the rotating disk versus the conductance ratio (Fig. 16) which falls by 50% between $k = 0$ and $k = 0.1$.

The streamlines for the current density are represented on Fig. 14 for the intermediate value $k = 0.1$, the origin of the stream function is taken at the axis of the cavity ($r = 0$). For $k \geqslant 10^{-3}$ all the lines enter the rotating disk and close in the fluid media via the lateral wall, with proportions which varies significantly with k (Fig. 17). When k is high enough most of the lines come back through the bottom wall (see Fig. 7 for $k = \infty$). For $k \geqslant 10^{-3}$ the electric flux through the rotating disk, which is the total electric current I_t, is then given by

$$I_t = \Delta\Psi = \Psi_{r=1} - \Psi_{r=0} = b_\theta(r = 1). \tag{39}$$

Using (29) we find a relation between the gradient at the rotating disk and the total electric current produced

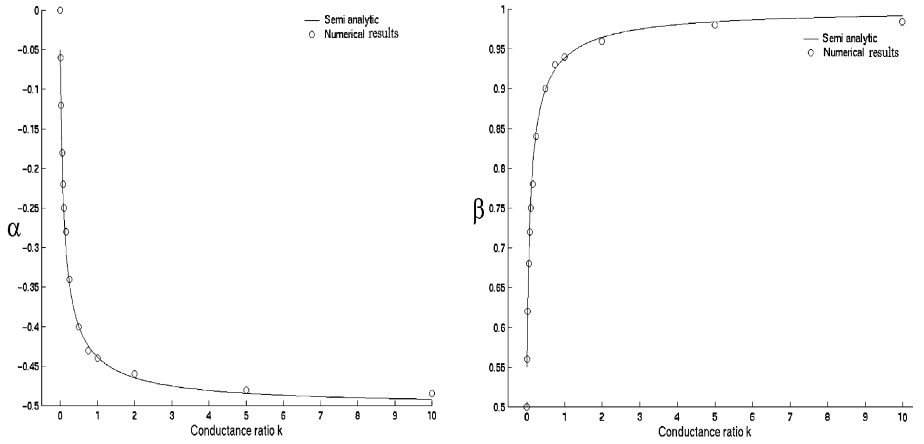

Fig. 15. Comparison between numerical and analytical results of α and β for $0 < k \leqslant 10$ at $r = 0.5$ ($Re = M = 100$). An interpolation for $k = 0$ can be deduced from the curves and gives $\alpha = 0$ and $\beta = 1/2$ for high M.

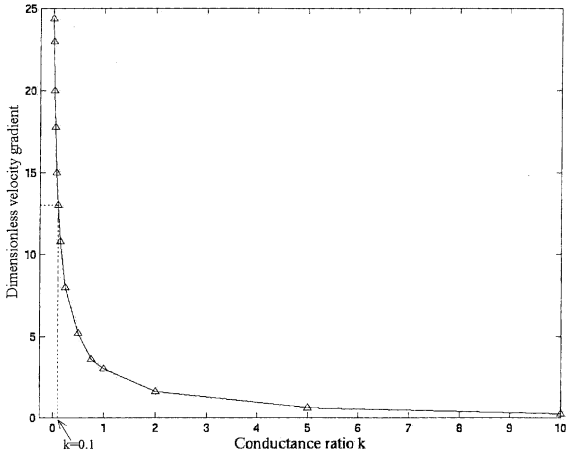

Fig. 16. Evolution of the average of the azimuthally velocity gradient over the surface of the rotating disk versus the conductance ratio k.

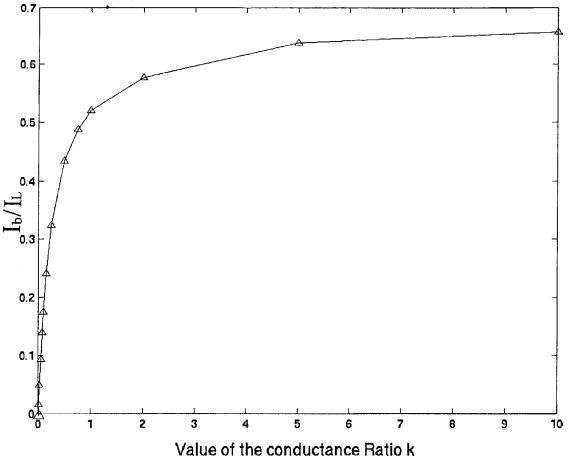

Fig. 17. Ratio of the electric current closing through the bottom wall I_b, over the one closing by the lateral wall I_L.

$$\frac{\partial U_\theta}{\partial z} \sim \frac{I_t}{k}. \tag{40}$$

Fig. 18 confirms this relation for $k \leqslant 1$, confirming the fact that for small k most of the electric current is created inside the Hartmann layers. By considering Eq. (38) it can be observed that k and M^{-1} seems to play the same role for the two disks, when k and $M^{-1/2}$ play the same role for the side layer. These parameters represent respectively the electric contribution of the wall and of the layers for the closure of the electric current. For the same reason already mentioned for the parallel layer, the inverse value of the Hartmann's number can be interpreted as the conductance ratio coefficient of the Hartmann's layer compared to the core flow. Thus, the wall and the Hartmann's layer can be interpreted as two electric resistances in parallel. For very conducting walls most of the electric current is produced by the rotating disc, the Hartmann's layer contribution becomes small ($k \gg M^{-1}$), and the relation (40) is no more valid. It can be deducted from Eq. (36) that the coefficient β varies from $r/2$ for the insulating case, to r for perfectly conducting case (Fig. 9), and presents a strong variation when k vary from $k = 0$ to $k = 0.1$. Then, the case of very small conductance ratio cannot be approximated by the insulating walls. This comes from the fact that, for large value of the Hartmann's number, the Hartmann's boundary layer is also very small and consequently the part of the electric current which closes itself inside the layer is comparable to the part of the electric current which closes inside the wall. For the same reason, the perfectly conducting profile is almost reached

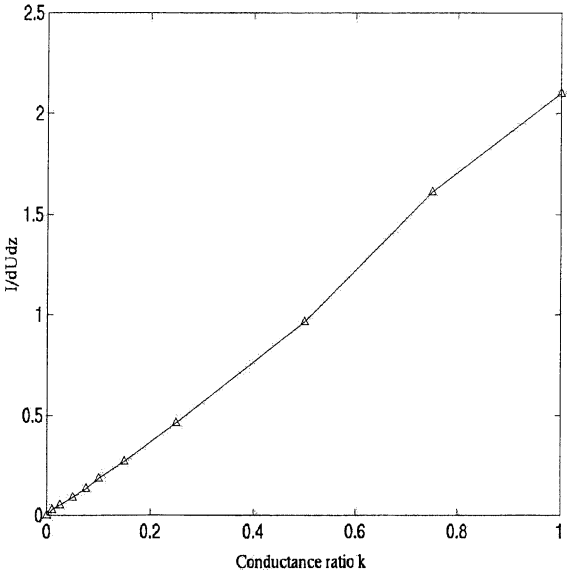

Fig. 18. The ratio of the total electric current to the average of the azimuthally velocity gradient at the rotating disk ($I_t/\frac{\partial U_\theta}{\partial_z}$) versus k.

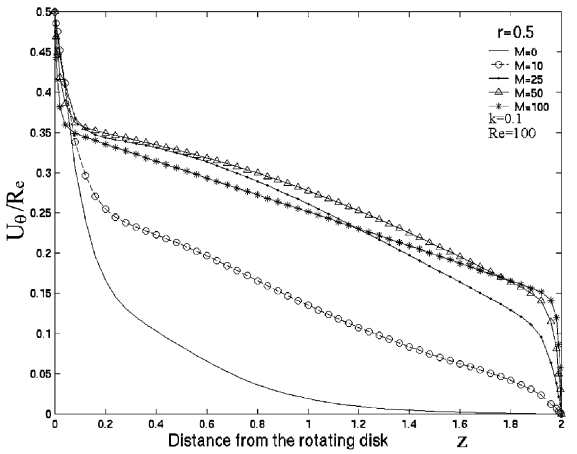

Fig. 19. Evolution of the azimuthally velocity versus the Hartmann number M for $k = 0.1$.

for $k > 0.5$. Even for small conductance ratio ($k = 0.1$) the evolution of the azimuthally component of the velocity versus the Hartmann's number described by Fig. 19 shows that the asymptotic solution for the insulating wall represented on Fig. 6 cannot be reached for $M = 100$. That's means that a significant part of the electric current closes through the wall. On the other hand, as demonstrated before, for asymptotic value of the Hartmann's number the conductance ratio k and $1/M$ plays the same role (see Eq. (38)). According to Fig. 20 which compare the effect of M and k for a given value

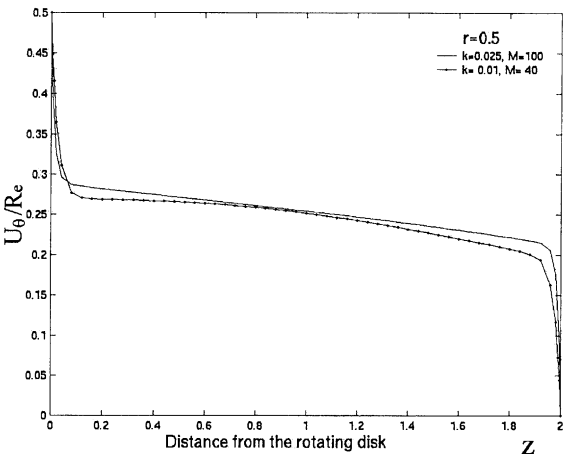

Fig. 20. Comparison of the azimuthally velocity distribution for two cases characterised by the same value of $k + 1/M$ ($Re = 100$).

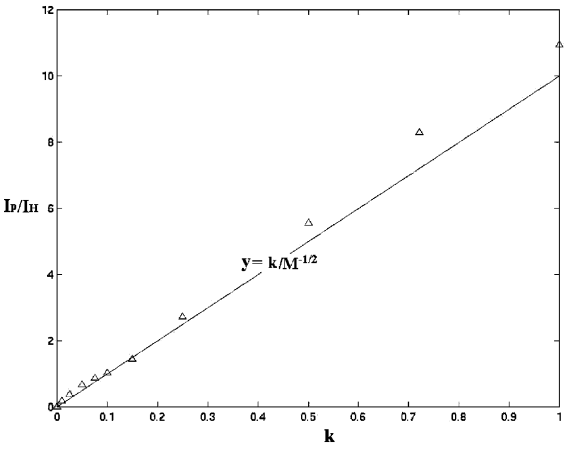

Fig. 21. Ratio of the total electric current circulating in the lateral wall I_p to that circulating inside the parallel layer I_H at midheight between the rotating disk and the bottom disk ($r = l, z = 1$), versus k ($M = 100$).

of the sum $k + (1/M)$, this property is well verified. Fig. 21 prove that the repartition of the electric current circulating inside the parallel wall parallel layer is controlled by the ratio between their own conductance ratio k/M^{-1}. Thus, the relation (35) is validated.

The meridian flow is now interpreted. Under the condition of axial symmetry, it controls the heat and mass transfer. The streamlines (Fig. 22) are plotted in the plane (r, z) for different values of the conductance ratio. It can be observed that the flow rate leads to be more homogeneously distributed in the central region as the conductance ratio increases. This is an other consequence of the fact that, as explained before, when k is

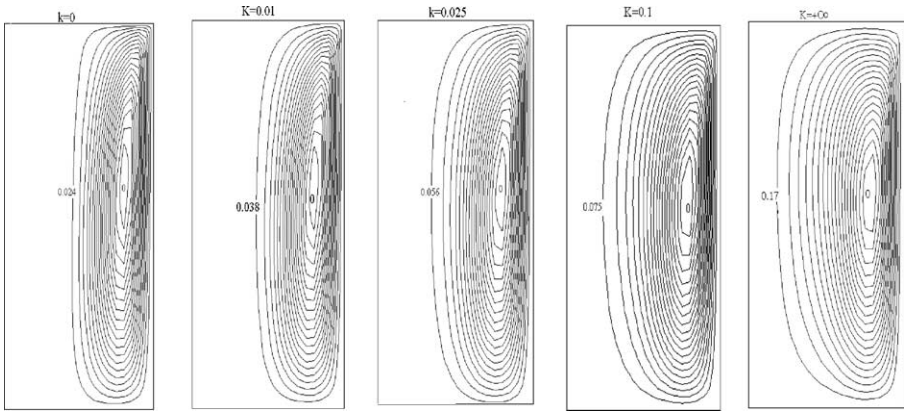

Fig. 22. Velocity streamlines for different values of k ($M = Re = 100$).

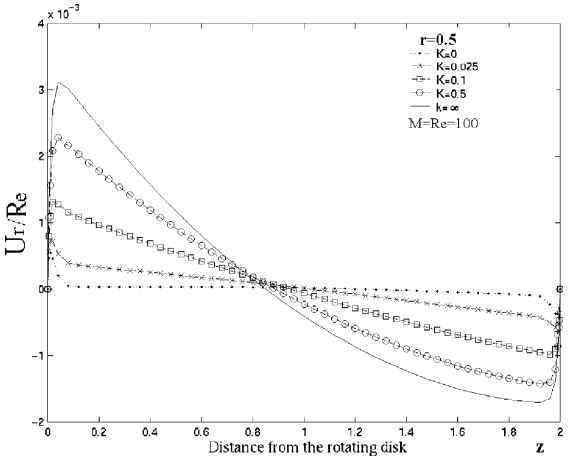

Fig. 23. Evolution of the radial velocity along the $r = 0.5$ line, plotted for different values of the conductance ratio ($M = Re = 100$).

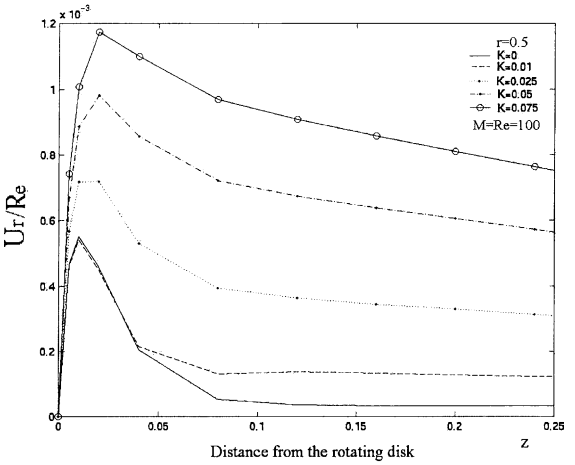

Fig. 24. Evolution of the radial velocity just under the rotating disk, plotted along $r = 0.5$ for small values of k. The velocity of the jet increases with k, but slower than the core radial velocity. When $k = 0.075$ the jet structure has almost disappeared.

increasing, the electric current lines become more and more parallel to the applied magnetic field direction. Another interpretation is that, when k is increasing, the electric current density inside the liquid increases also. Then all the deviation from a vertical motion of the flow in the central region generates an electromagnetic counter reaction opposite to this deviation that increases when the electric current density increases. Consequently, the fluid particles follow the imposed magnetic lines regularly disposed. Due to the fact that the azimuthally velocity increases in the core flow when both the magnetic field and the conductance ratio increases, the radial velocity also increases and then the jet structure of the radial flow disappears and is replaced by a regular curve on the full domain (Figs. 23 and 24). Nevertheless, the radial component of the Lorentz force $F_r = -M^2 \cdot U_r$ being opposite to the radial flow the radial velocity should be much smaller than the azimuthally velocity. The main mechanism responsible of the flow rate is the centrifugal force. In the upper Hartman's layer this force creates a high zone pressure at the periphery of the rotating disk. This high pressure is responsible for the closure of the flow through the side layer and the bottom Hartmann's layer. Out of the side layer, the pressure is almost constant in the axial direction (Fig. 25); this property will be demonstrated later.

As explained before, the jet structure of the radial flow just under the disk, directed towards the lateral wall, disappears when the Hartmann number increases. The maximum of the velocity V_r^j depends on equilibrium between the viscous and centrifugal force that gives

$$\frac{\partial^2 U_r}{\partial z^2} \sim \frac{U_\theta^2}{r} \Rightarrow \frac{V_r^j}{\delta^2} \sim U_\theta^2 \Rightarrow V_r^j \sim \left(\frac{\beta}{M}\right)^2. \tag{41}$$

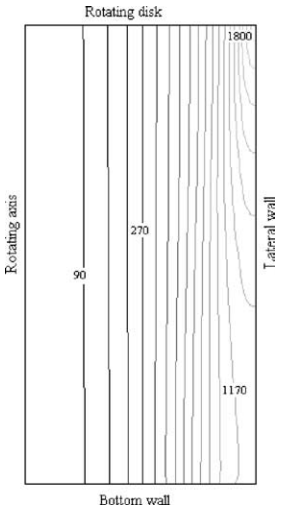

Fig. 25. Distribution of the pressure for $k = 0.1$.

Thus, according to (41), V_r^j should increase as $(\beta/M)^2$.

The high pressure zone at the corner of the rotating disk imposes a flow rate along the side wall. Characterised by an Hartmann parallel layer corresponding to an equilibrium between the vertical pressure gradient and the viscosity when the radial pressure gradient is controlled by electromagnetic and centrifugal forces. The pressure decreases from the corner of the rotating disk to the corner of the fixed disk.

In the bottom Hartmann layer the centrifugal force is reduced and, under the influence of the radial pressure gradient, the fluid moves toward the centre of the fixed disk. This motion corresponds to an equilibrium between the electromagnetic and the pressure gradient forces. The flow in this region has the same configuration as under the rotating disk, its amplitude is a little lower but conserves nevertheless the same order of magnitude, as can be deduced from the simple relation

$$\frac{\partial P}{\partial r} \sim M^2 \cdot U_r \sim \beta^2. \tag{42}$$

For a constant Hartmann number the radial pressure gradient increase when β^2 increases therefore when k increases (Fig. 26). The axial (i.e. vertical) velocity is connected to the radial velocity by the continuity equation (14), its order of magnitude inside the Hartmann layers is

$$U_z \sim \frac{U_r}{M}, \tag{43}$$

and conserves the same order of magnitude in the core flow. The distribution of the axial velocity as a function of k is shown on Fig. 27. Note that U_z increases with k. This is in accordance with the previous remark

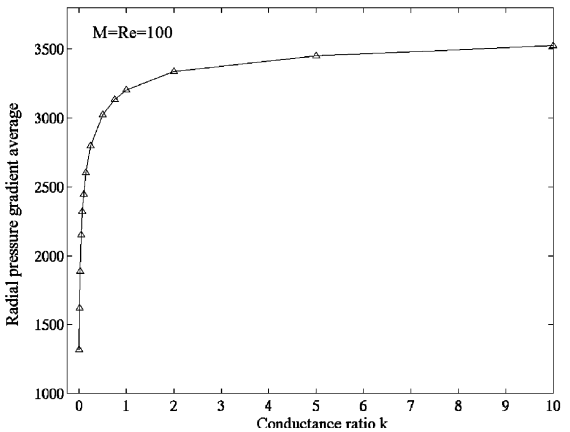

Fig. 26. Evolution of the average of the radial pressure gradient $\frac{\partial P}{\partial r}(z = 0)$ over the rotating disk versus the conductance ratio k.

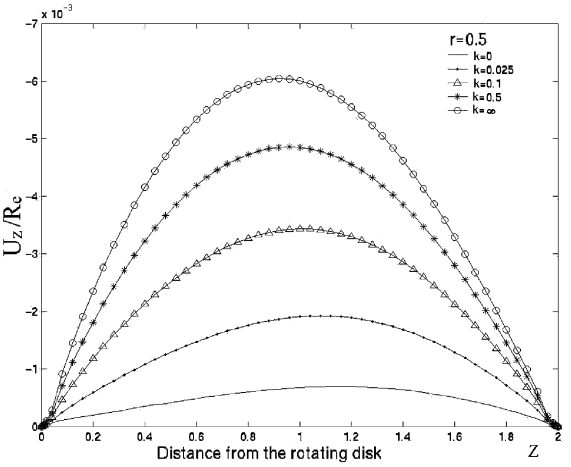

Fig. 27. Evolution of the axial velocity along the $r = 0.5$ line, plotted for different values of the conductance ratio ($M = Re = 100$).

explaining that k and $1/M$ play the same role and consequently, Fig. 27 results are in accordance with Eq. (43). By knowing the order of magnitude of U_z in the core flow, it is easy to deduce the axial pressure gradient necessary to maintain this velocity value. This can be achieved from Eq. (12) by neglecting the viscosity

$$\frac{\partial P}{\partial z} \sim U_z^2 \sim U_r^2. \tag{44}$$

The axial pressure gradient is M^2 smaller than the radial one from 42. It can be concluded that in the core flow the iso-pressure lines are almost vertical as shown in Fig. 25. In all the cases the flow rate is at least Hartmann time smaller than the ones generated by Ekman pumping ($B_0 = 0$). The magnetic field should decrease the heat and mass transfer from the rotating disk to the cavity.

4.4. The vortex breakdown

The occurrence of vortex breakdown phenomena is a typical property of this kind of flow and appears for small Reynolds number ($Re = O(10^3)$) while it occurs at higher value of Re and swirl number in aeronautics. In laminar flows, Escudier [16] determinated experimentally the conditions under which breakdown occurs. For the case of the present paper the calculations show that the vortex appears at $Re \approx 1454$ and disappears at $Re \approx 3020$, while between $Re \approx 1830$ and 2283, there is two vortex. This is in total accordance with Escudier. The appearance of the vortex is not completely understood.

The influence of the magnetic field on the vortex breakdown phenomena has not been yet investigated. But as it can be predicted, as usual, the magnetic field tends to suppress the non-homogeneities and then it can be expected a disappearance of the vortex for large Hartmann number. Fig. 28 represents the critical Hartmann number M_k for which the principal vortex is suppressed, for different values of the conductance ratio k. The secondary vortex disappears for any value of Re and k at $M \approx 5$. The evolution of the critical Hartmann number, characterised by the curve $M^k = f(Re)$, shows an increasing as $\beta(Re)^{1/2}$ order. In other words the vortex disappears for higher value in the case of conducting wall than the insulating wall. An other surprise is connected with the existence of an electric vortex breakdown at the same location than the hydrodynamic one Fig. 29. It seems that this electric vortex is not correlated with the hydrodynamics one because the modification of the electric stream lines due to the hydrodynamics vortex is tangentially directed, when the electric vortex is located in the meridian plan. This electric vortex appears immediately for $M > 0$ and disappears for critical Hartmann number $M \approx M^k + 5$. It exists only in the range of Re corresponding to the hydrodynamic one but is maintained for higher values of M. No electric secondary vortex was found. These two vortexes (hydrodynamics and electric) seem to have the same origin. According to the induction equation (14), the source of the creation of these vortex is due or connected with the axial gradient of the azimuthally velocity $\frac{\partial U_\theta}{\partial z}$. This confirms the assumption of Brown and Lopez [17] that argued that the change of sign of $\frac{1}{r^3} U_\theta \frac{\partial U_\theta}{\partial z}$ near the axis of the cylinder is responsible for the appearance of the vortex. More recently Gelfgat et al. [18] have shown that the change of sign condition is necessary but not enough.

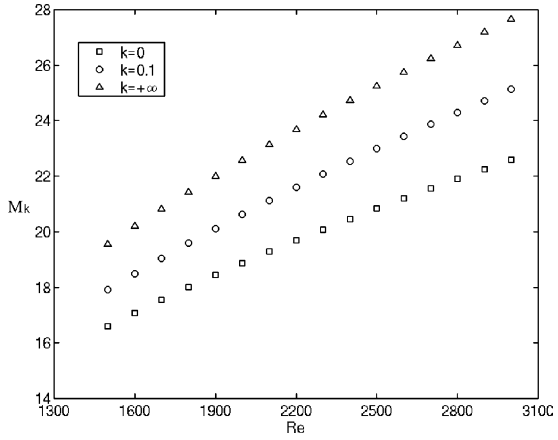

Fig. 29. Evolution of the critical Hartmann number M^k for which the hydrodynamic vortex breakdown disappear versus the Reynolds number.

4.5. The mass transfer

Corrosion studies have shown that the structural materials (austenitic and martensitic steels) exposed to high temperature Pb–17Li are subjected to corrosion.

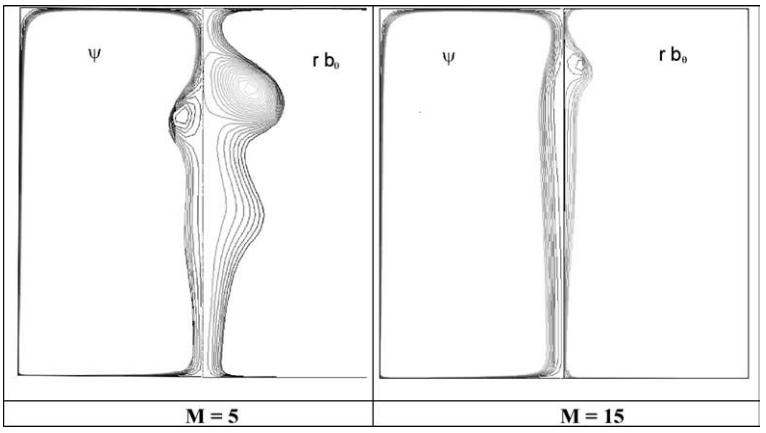

Fig. 28. Shape of the hydrodynamic (Ψ) and electric (rb_θ) vortex breakdown for two different Hartmann number for $Re = 1750$.

From studies carried out in flowing lead–lithium alloy, it is known [19] that corrosion rate of martensitic steels, increases from 21 to 93 $\mu m\,yr^{-1}$ when the alloy velocity increases from 0.019 to 0.18 $m\,s^{-1}$. This constatation leads us to think that the corrosion process is controlled by the near-wall hydrodynamic. It has to be noted that the knowledge of the diffusion coefficient as well as the solubility of the dissolved species in the liquid is essential for the modelling. Experiences with steel rotating disk are planed, different situation with different velocity and different magnitude of magnetic field will be tested. The diffusion coefficient D of metallic element could be deducted from these experiences. A precise modelling of mass transfer is nevertheless necessary for a correct interpretation of the experimental results. For the present study the Schmidt number ($Sc = \nu/D$) is 1000, the diffusion layer thickness is then at least one order of magnitude smaller than the hydrodynamical one. A supplementar grid refinement is then necessary to define correctly the concentration boundary layers.

The equation of the concentration of metallic element is computed over all the domain:

$$U_r \frac{\partial C}{\partial r} + U_z \frac{\partial C}{\partial z^*} = \frac{1}{Sc} \Delta C. \tag{45}$$

The boundary conditions are $C = 1$ at the rotating disk, $C = 0$ for the other walls, and $\frac{\partial C}{\partial r} = 0$ at the axis.

The mass flux is defined through the classical Sherwood number

$$Sh(r) = \frac{\mathrm{Flux}(r)}{Sc C_{\mathrm{ref}}},$$

where

$$\mathrm{Flux}(r) = -\frac{1}{Sc} \frac{\partial C}{\partial z} \quad \text{and} \quad C_{\mathrm{ref}} = 1. \tag{46}$$

4.5.1. Influence of the Reynolds number

The mass transfer in this case have been deeply investigated. Our calculations give for the total flow of matter from the rotating disk:

$$Sh(R) = 2.6(Re)^{1/2}(Sc)^{1/3}. \tag{47}$$

This is in good agreement with what can be found in the literature [20].

4.5.2. Influence of the Hartmann number and conductance ratio

Studies on the effects of an external magnetic field on the mass transfer can be found in literature. They are mostly connected with the crystal growth in which the transfer is not controlled only by the conduction and the convection. In these studies there is not equivalent aspects concerning the influence of the conductance ratio on the mass transfer processes.

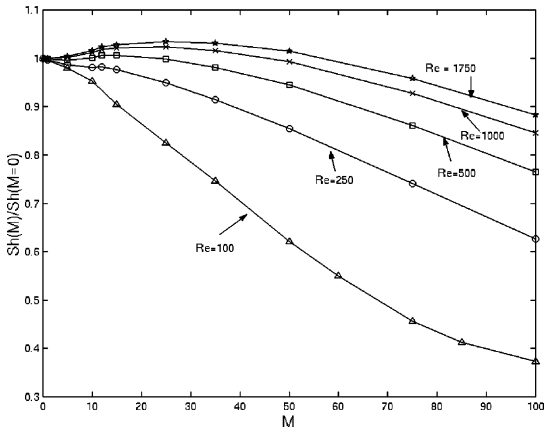

Fig. 30. Evolution of the total mass transfer through the rotating disk versus M for different Reynolds number ($k = 0$).

In the particular conditions of the present study the magnetic field action results in a decreasing of the forced convection, then the mass transfer is expected to be much smaller than in the case without magnetic field. This cannot be take as a general conclusion. In other circumstance the magnetic field action on hydrodynamics could improve on the contrary the mass transfer rate. Fig. 30 represents the ratio between the Sherwood number in presence of magnetic field and insulating wall, over the one without magnetic field. This ratio can be expressed on the form:

$$Sh(M)/Sh(M = 0) \approx f(M, Re) \mathrm{e}^{-M/R_e} \tag{48}$$

with $0.9 \leqslant f(M, Re) < 1.06$. No analytic general expression for $f(M, Re)$ was found. As expected the curves decrease exponentially with M. For small $Re (Re \ll M^2)$ the magnetic field seems to increase a little bit the mass transfer. For $Re = 1750$ the correlation (48) gives $Sh(M = 25)/Sh(M = 0) \approx 1.04$. This can be only associated with an increasing of the flow rate in the boundary layer corresponding to an improvement of the flow rate which supply the boundary layer. That means that, since $Q \sim \delta(Re, M) U_r$, the product $\delta . U_r$ is improving for small value of M. This can be justified by the following simple explanation. The radial Lorentz force ($-M^2 U_r$) act in the same direction that the viscous force inside the rotating disk boundary layer, which is characterised roughly by the equilibrium:

$$\frac{\partial^2 U_r}{\partial z^2} - M^2 U_r \sim \frac{U_\theta^2}{r} \tag{49}$$

consequently, at the first order:

$$\frac{U_r}{\delta^2} - M^2 U_r \sim U_\theta^2 \tag{50}$$

assuming that for small $M (M^2 \ll R) e$, $U_\theta \sim Re$, the boundary layer depth is $(Re)^{-1/2}$. Using (50), the flow rate can be expressed on the form:

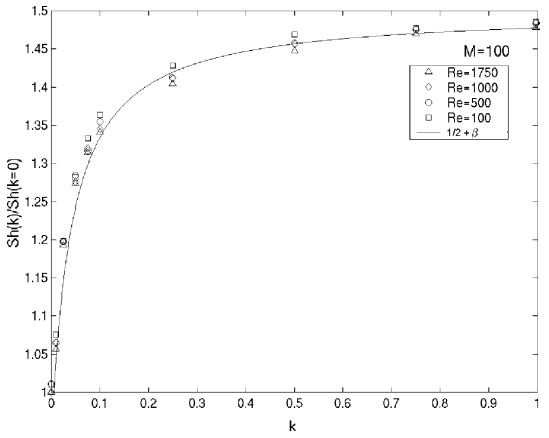

Fig. 31. Evolution of the total mass transfer from the rotating disk versus k for different Reynolds number ($M = 100$).

$$Q \sim \delta U_r \sim \frac{Re}{(1 - M^2/Re)}. \tag{51}$$

This relation, found for very small M, justify the increasing of the flow rate for an increasing of the Hartmann number.

The variation of Sh versus k is given in Fig. 31 for MHD case ($M^2 > Re$), the following relation is found:

$$Sh(k)/Sh(k = 0) \approx (1 + 2\beta)/2. \tag{52}$$

Finally:

$$Sh = (1 + 2\beta)\mathrm{e}^{-M/Re} Sh(M = 0)/2. \tag{53}$$

As can be observed the mass transfer is greatly enhanced when the electrical conductivity of the walls increases. This is because the dominant mode of transfer here is convection and the velocities which are responsible for this transfer are progressively dampened as one changes from the fully conducting case to the totally insulating case.

5. Conclusions

Corrosion experiments in liquid Pb–17Li under a magnetic field are planned with flows generated in a cylindrical cavity by a rotating disk. In order to correlate mass transfer and hydrodynamics in such configuration, the velocity distribution has to be known. A numerical analysis based on the induced magnetic field and using a thin wall hypothesis has been carried out to predict the flow. The calculations for large values of the conductance ratio k indicate that the hydrodynamics is largely controlled by this factor. Even for very small values of k, the wall cannot be assimilated to be insulating case when the Hartmann number is high enough when, even for $k < 1$ ($k > 0.5$ for $Re = 100$), the flow is very close to the perfectly conducting case ($k = \infty$). This can be easily explained by the sharing of the electric current between the walls, and the Hartmann and parallel layers. Depending on the thickness of the wall (taken into account by the conductivity ratio) and the thickness of the boundary layers ($1/M$ and $1/M^{1/2}$ plays the role of the conductance ratios for the two layers), the electric current closes preferentially inside the wall or inside the layers. For large values of M, the two layers are very small and then the current closes preferentially in the walls even if they are very thin. In conclusion, the two products kM and $kM^{1/2}$ control the situation. When $kM \ll 1$ the two disks (rotating and fix) can be considered as insulating and in the same way, when $kM^{1/2} \ll 1$ the lateral walls can also be considered as insulating. Consequently an intermediate situation is possible with the two disks considered as perfectly conducting while the lateral walls are considered as insulating. Fig. 32 summarizes the different situations.

The azimuthally velocity is classically organized into core, Hartmann layers, and a parallel layer. The core flow exhibits a linear velocity variation in the axial direction, with a slope that depends strongly on k. The boundary layers thickness is constant with k, but the azimuthally velocity gradient at the rotating disk (and thus the mass transfer process) varies considerably with this factor. The electric current lines are parallel to the imposed magnetic field in the core flow, and at the vicinity of both disks for the perfectly conducting case. Thus, the vanishing of the Lorentz force explains why the meridian flow rate is stronger for high k.

Numerical simulations of mass transfer, for high Schmidt number, from the rotating disk in laminar flow show that magnetic field changes significantly the phenomena. Although the presence of the magnetic field in

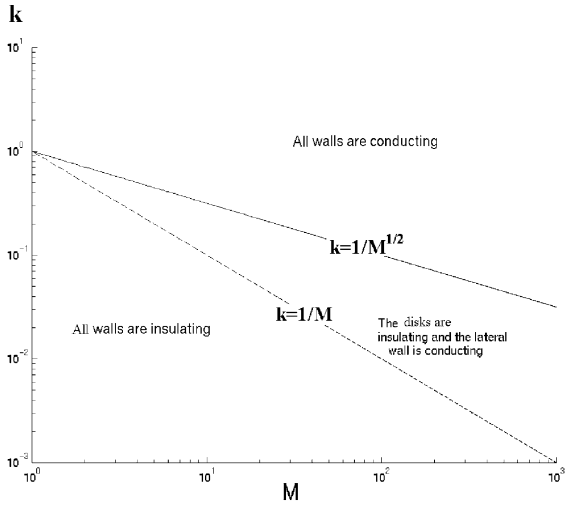

Fig. 32. Characteristic situations versus the conductance ratio and the Hartmann number.

the present geometry damp the mass transfer, in the case of the ducts of the blanket for the fusion reactor, the mass transfer could be increased due to a strong modification of the hydrodynamics inside the duct. This is characterised by a relatively high velocity at the vicinity of the wall and lower velocity in the core flow corresponding to an improvement of the mass transfer that is controlled by the near-wall hydrodynamics. The objective of the experimental results that will follow this study will be only to control the dependence between the mass transfer rates with the modification of hydrodynamics of the flow. The electric properties of the walls, through the conductance ratio k, play a significant role in the mass transfer. So, if the corrosion processes is controlled by the near walls hydrodynamics, the conductance ratio of the walls is an important factor which cannot be neglected.

Acknowledgements

The author wish to thank E. Pierson from university of Chicago, for his help during the redaction of this paper.

References

[1] A. Terlain, T. Dufrenoy, Influence of a magnetic field on the corrosion of austenitic and martensitic steels by semi-stagnant Pb–17Li, J. Nucl. Mater. 150 (1994) 212–215.
[2] S. Mori, K. Satoh, A. Tanimoto, Electrolytic mass transfer around inclined cylinders in static magnetic field, Electrochim. Acta 18 (1994) 2789–2794.
[3] S. Mori, K. Satoh, A. Tanimoto, Enhancement of electrolytic mass transfer around spheres by applying static magnetic fields, J. Chem. Eng. Japan 27 (6) (1994) 803–807.
[4] S. Mori, M. Kumita, M. Takeuchi, A. Tanimoto, Effect of pulsating magnetic fields on electrolytic mass transfer around cylindrical cathodes, J. Chem. Eng. Japan 29 (1996) 229–234.
[5] J.S. Walker, M.G. Williams, Effects of the crystal's non-zero electrical conductivity on the rotationally driven melt motion during Czochralski silicon growth with a uniform, transverse magnetic field, J. Cryst. Growth 132 (1993) 31–39.
[6] R.W. Series, D.T.J. Hurle, The use of magnetic fields in semiconductor crystal of growth, J. Cryst. Growth 113 (1991) 305–310.
[7] P.F. Thomlan, J.L. Hudson, Flow near an enclosed rotating disk: analysis, Chem. Eng. Sci. 26 (1971) 1591–1600.
[8] W.S. Lewellen, Review of Confined Vortex Flows, Space Propulsion Laboratory, MIT, Cambridge, Massachussetts, 1971.
[9] E. Lang, K. Sridhar, N.W. Wilson, Computational study of disk driven rotating flow in a cylindrical enclosure, J. Fluids Eng. 116 (1994) 815–820.
[10] J.W. Daily, R.E. Nece, Chamber dimension effects on induced flow and frictional resistance of enclosed rotating disks, ASME J. Basic Eng. 82 (1960) 217.
[11] R. Bessaih, P.H. Marty, M. Kadja, Numerical study of disk driven rotating MHD flow metal in a cylindrical enclosure, Acta Mech. 135 (1999) 153–167.
[12] L. Hjellming, J.S. Walker, Melt motion in a Czochalski crytal puller with an axial magnetic field: isothermal motion, J. Fluid Mech. 164 (1986) 237–273.
[13] S. Molokov, Fully developed liquid metal flow in multiple rectangular ducts in a strong magnetic field, Eur. J. Mech. B—Fluids 6 (1993) 769–787.
[14] U. Müller, Liquid metal blanket concept for a fusion reactor and related MHD research, in: Proceedings of the International Conference Energy Transfer in Magnetohydrodynamics Flows, vol. 1, Aussois, France, 1994, pp. 359–364.
[15] L. Leboucher, Monotone scheme and boundary conditions for finite volume simulation of MHD internal flows at high Hartmann number, J. Comput. Phys. 150 (1999) 181–198.
[16] Escudier, Observation of the flow producd in a cylindrical container by a rotating endwall, Exps. Fluids 2 (1984) 189–196.
[17] G.L. Brown, Lopez, Axisymmetric vortex breakdown. Part 2. Physical mechanisms, J. Fluid Mech. 221 (1990) 533–576.
[18] Gelfgat, Bar-yoseph, Solan, Stability of confined swirling flow with or without vortex breakdown, Journal of Fluid Mechanics 311 (1990) 1–36.
[19] J. Sannier, T. Flament, A. Terlain, Fus. Technol. 901 (1994).
[20] H. Schlichting, Boundary-Layer Theory, seventh ed., McGraw-Hill, New York, 1988.